Salem *et al. Herit Sci* (2019) 7:19
https://doi.org/10.1186/s40494-019-0261-2

Heritage Science

RESEARCH ARTICLE Open Access

Characterization of the microstructural features and the rust layers of an archaeological iron sword in the Egyptian Museum in Cairo (380–500 A.D.)

Yussri Salem[1*], Omid Oudbashi[2] and Doaa Eid[3]

Abstract

In this paper, a sword is investigated from a collection of archaeological iron swords displayed in the Egyptian Museum from the civilization centered on Ballana and Qustul in Egyptian Nubia (380–600 A.D.). A range of metallographic analytical techniques have been used to characterize the sword's metallic structure and its rust crust. The results revealed that the sword was made of low-carbon steel and corrosion products formed on the surface are iron sulfate, iron oxides/hydroxides including goethite, maghemite, magnetite, lepidocrocite, akaganeite and ferric chloride. The investigation also revealed that the rust crust constituted of two corrosion layers: a dense layer and a transformed medium. Crystals of soil minerals were clearly observed in the outer corrosion layer. Moreover, several microstructural features were detected, indicating the stage of deterioration and the features of metallurgy of this sword. Furthermore, the obtained results have been used to select appropriate conservation procedures for preventing degradation in the future and ensuring its reliable restoration.

Keywords: Egyptian Nubia, Archaeological Sword, Iron, Rust, SEM, XRD

Introduction

As a weapon, the sword first appeared as a simple long dagger made of tin bronze in ancient Egypt [1, 2]: even the swords used in the battle of Kadesh in 1274 BC were made of bronze [1, 3]. The long dagger shape sword developed into the sickle sword or *Khopesh*, which is characterized by a curved thick blade. With this shape, the *Khopesh* became one of the most important weapons in the ancient Egyptian army [2, 4, 5]. It continued to be made of bronze until the Iron Age which began in the Egypt at the eighth century BC. In ancient Egypt, Some iron artifacts were made of meteoritic iron before that time which shows the knowledge of how to extract iron from its ores [6–9].

In Nubia, iron was not known before the sixth century BC [10]. Nubia was a large region located on the river Nile covering southern Egypt and northern Sudan. Archaeologists have divided Nubia into three civilizations: Napatan, Meroitic and X-group (Ballana and Qustul) [10]. The X-group civilization is located in the Ballana and Qustul villages in Egyptian lower Nubia (Fig. 1) and dates to around 350–600 AD in the time after the collapse of the Meroitic state and before the founding of the Christian Nubian kingdoms [11]. This civilization was unknown until October 1931 when two archaeologists (Walter Emery and Lawrence P. Kirwan) began an expedition in the tumuli of Ballana and Qustul. By November 1931, remains of sacrificial horses were found [10, 11]. At the end of their expedition in 1934, they discovered many royal tombs which were equipped with the richest funerary goods in Nubia. Bronze, iron and silver artifacts such as spears, axes, chisels and hammers were found in these tombs [12].

*Correspondence: Yousry.ali@arch.svu.edu.eg
[1] Conservation Department, Faculty of Archaeology, South Valley University, Qena 83523, Egypt
Full list of author information is available at the end of the article

Springer Open

© The Author(s) 2019. This article is distributed under the terms of the Creative Commons Attribution 4.0 International License (http://creativecommons.org/licenses/by/4.0/), which permits unrestricted use, distribution, and reproduction in any medium, provided you give appropriate credit to the original author(s) and the source, provide a link to the Creative Commons license, and indicate if changes were made. The Creative Commons Public Domain Dedication waiver (http://creativecommons.org/publicdomain/zero/1.0/) applies to the data made available in this article, unless otherwise stated.

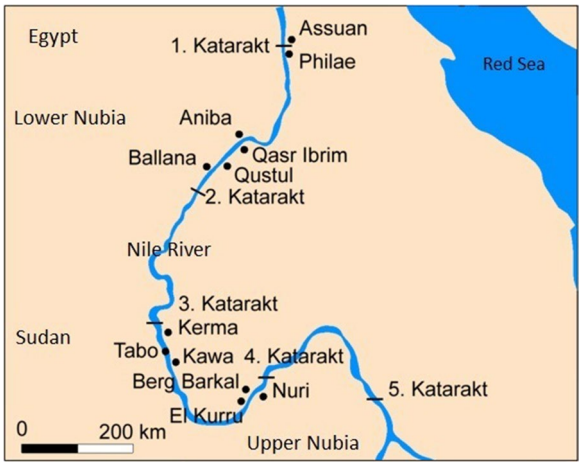

Fig. 1 Map showing Ballana and Qustul in the south of Egypt in Lower Nubia [10]

Study on iron technology in the archaeological iron objects produced in the ancient time has been an interesting subject during the last decades. For example, a large number of studies are performed to analysis of chemical composition and microstructure of archaeological irons to show the technology of iron production and manufacturing of iron objects around the world by using various analytical and microscopic methods [6, 8, 9, 13–18]. These variable studies have led to characterize the methods of production of different iron alloys in the ancient time with variable microscopic and microscopic characteristics. On the other hand, the corrosion mechanism and morphology of the archaeological iron artifacts has been the subject of many researches during the twentieth and twenty-first centuries. The study on corrosion occurred in the archaeological iron objects has helped the scientists to understand the physico-chemical events that led to corrosion in the buried iron alloys as well as to conservators to characterize decay mechanism and to control the deterioration in the excavated iron objects [19–26]. It shows obviously that the technology and corrosion of archaeological iron objects is an important subject for scholars from various disciplines, especially when the results lead to preserve these types of cultural heritage objects.

The present paper aims to study an iron sword discovered from the Egyptian Nubia by using various laboratory methods. There are no data about the metallurgy of steel in that civilization, it is important to find some literature about the metallurgy of steel making in the region in that time. Also, it is important to note that there is no analytical study in this field. Thus, it is necessary to conduct more studies on this subject in the future. It is worth noting that the current study is one of the early analytical case study works on the iron production and corrosion in the Nubian civilization and can be considered as a pioneer work to develop analytical study in this field. Regarding the appearance of the sword, it is necessary to investigate the metallurgical aspects of the sword including the composition and microstructure by microscopic/microanalytical and analytical methods. Therefore, this research deals with the different characteristics of the Egyptian iron sword currently displayed in the Egyptian museum in Cairo. In fact, this study also highlights the role of the examination and analysis of the metallic composition and microstructure, and corrosion layers to identify the conservation conditions and the decision-making to select appropriate treatment methods for the analyzed sword. The study also aims to understand the corrosion mechanisms of archaeological iron, especially low-carbon steel, in the long-term burial.

Materials and methods

Descriptions and visual examination

The study focuses on the analysis of an archaeological iron sword from old Nubia that now is displayed in the Egyptian Museum in Cairo (No. 234). The sword is very straight and lengthy, at approximately 150 cm long. The thickness clearly increased and varied from area to another (Fig. 2).

Visual examination reveals that the sword was subjected to various corrosion processes and was heavily deteriorated. It was completely covered with a thick crust of corrosion products with various colors. Several features of damage were detected including: solid globular masses of corrosion products mixed with soil deposits, a clear increase in thickness of the sword as a result of formation of the rust layer, and fracture in the hilt and loss in two zones. The outer corrosion layer on both sides is very rough and included on swilling, exfoliation, flaking and pitting phenomena. These deterioration features indicate the probable aggressive/corrosive conditions of the burial environment. The border of the original surface may has been lost and a change in shape and thickness has occurred in the sword structure. The sword has a long hilt and more than its half is covered with a silver sheet. The hilt is corroded more than the blade, especially in the part under the silver sheet. The sword has lost some parts of its metallic structure and has become very fragile and brittle (Fig. 2). A white coating layer was observed on the surface. The appearance and texture indicate that this layer may be a protective layer applied during previous conservation procedures.

Preparation of the cross-sections

Two metallographic samples were taken from the edge of the sword for preparing a cross-section to study of the metallic structure and the rust crust. The specimens were prepared according to standard metallographic procedures as follows [26]: they were mounted in two-part epoxy resin, grounded using SiC papers (grade from 1000 to 4000) without using water and then polished with diamond paste 0.25 µm. After elemental analysis of the metallic structure and Raman analysis of the different corrosion layers, the polished sections were etched with Nital solution (100 ml ethanol and 2 ml nitric acid) for further metallographic studies.

Chemical composition of the metallic structure

As noted above, the sword is completely covered by a thick rust layer and its metallic core is obscured under this layer, therefore the elemental analysis should be carried out using scanning electron microscopy coupled with energy-dispersive X-ray spectroscopy (SEM–EDS) method. The analysis was performed at central metallurgical research and development institute (CMRDI) in Cairo, Egypt by the method of X-ray energy-dispersive spectroscopy (EDS) using INCAPentaFETx3 spectrometer with power: 30 kV, Si(Li) detector, and JEOL (JSM-5410 model) scanning electron microscope (SEM). The EDS analysis performed here can not quantify light elements such as carbon [27]. This element is especially important to the study of archaeological iron samples because they usually contain various concentrations of carbon. Thus, it was also necessary to perform another type of elemental analysis, and for this purpose, a carbon sulfur analyzer was used to determine the carbon concentration if found and thus to determine the type of iron alloy. The analysis was carried out at CMRDI and the parameters were as follows: the model: ELTRA's CS-2000, detection method: solid state infrared absorption, Number of IR cells, 1–4: Material of IR path: gold, time of analysis: 40 s, compressed air: 4 bar/60 psi, and power: 230 V, 50/60 Hz, max. 15 A, 3450 W.

Elemental analysis of the silver sheet of the sword hilt was conducted by portable X-ray fluorescence (pXRF) using modal Elio XGlab's company, the device is existing at the Egyptian museum of Cairo and the analysis directly carried out on the surface without taking sample. The analysis parameters were as follows: measurement time: 40 s, tube voltage: 40 kV, tube current: 20 µA, spectrum left cut: 1 keV, spectrum right cut: 50 keV, spectrum upper limit: 50 keV. Analysis by pXRF of thirteen spots on the sword surface was also performed. The sword's surface was mineralized so the purpose of the elemental analysis is not to identify the metallic core. The analysis by pXRF of many points on the corroded surface may recognize some elements that are not attributed to the defined corrosion products by the Raman.

Mineral composition analysis

Three samples of the corrosion layer were powdered using an Agate mortar and were analyzed. The analysis conducted to CMRDI with an X-ray diffractometer, Bruker D8 advance using CuKα radiation, calibrated against a quartz standard and wavelength of 1.789 Å. Raman analyses were also used to identify the internal corrosion layers. Raman measurements were carried out in Egyptian Petroleum Research Institute (EPRI) Cairo via dispersive Raman microscope: model Senterra, Bruker. Spectra were acquired with wavelength of 785 nm, laser power 5 mW, aperture setting 50 × 1000 µm and the sample was scanned twice. The spectrometer calibration is obtained from a silicon crystal which the Raman signal is at 520.5 cm^{-1}.

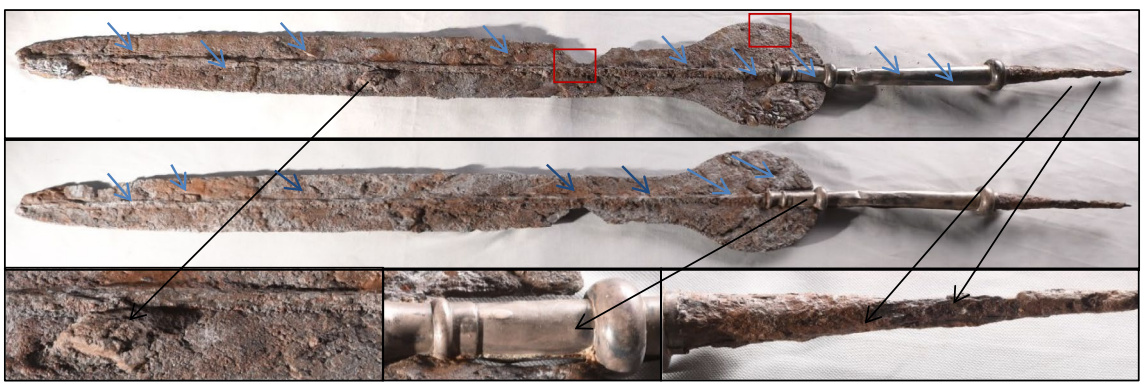

Fig. 2 Shows the sword from both the sides, some details of the hilt, the solid globular masses from soil deposits with corrosion products, the zones of the taken samples (the red boxes) and the analysis spots by pXRF on the surface (the blue arrows)

Microscopic characterization

The investigation of the corrosion layer and metallic structure were conducted on the samples of the polished cross-section before and after the etching. The characterization was performed by optical microscopy (OM) using polarized light microscope model Bx5 manufactured by Olympus Company, Japan, and scanning electron microscope (SEM). Also, the sword's surface was observed and examined in the Egyptian Museum Laboratory using low magnification by stereomicroscope model M60 magnification range 500× manufactured by Leica, Germany equipped with a leica MC 190 HD digital microscope camera.

Identify the coating layer

The coating layer was identified by Fourier-Transform Infrared spectroscopy (FTIR) method, by a FT-IR spectrometer model Jasco 4100, KBr disc as standard reference, resolution 4 cm^{-1}, scanning speed 2 mm/sec, detector TGS and wavenumber from 349 to 7800 cm^{-1}.

X-ray radiography

X-rays radiographic investigation was used to reveal the areas of corrosion layers and some areas of object that have lost the metallic structure and are partially mineralized. The examination was conducted in the Egyptian Museum Laboratory, the X-ray unit is model PXP-60HF and the X-ray parameters are 110 kV, 33 MA and 85 D.

Results and discussion

Microscopic observations

Examinations by stereomicroscope of the corroded sword surface shows the common shape of the goethite (α-FeOOH) corrosion product in iron artifacts, which is described as a 'cotton ball' shape [28, 29]. This shape appeared on the surface as yellow spots under corrosion products; these spots increase and expand until the external corrosion layer explodes and the yellow color appears as shown in Fig. 3a–d. Some areas of the artifact present different aspects of damage such as cracking, splitting and flaking on broken sections due to the volume increasing caused by the formation of goethite [28]. Other features revealed on the sword surface under low magnification are microscopic features such as deep cracks and shiny blisters most likely resulting from a corrosion phenomenon namely "weeping" (Fig. 3e–g) [19]. The white layer that was macroscopically observed was confirmed microscopically too (Fig. 3h).

Chemical compositions

The carbon/sulfur analyser and energy-dispersive X-ray spectroscopy revealed that the metallic matrix of the sword is of low-carbon steel [30], the main element is iron with impurities mainly consisting of carbon, silicon, aluminium, and phosphorus as shown in Fig. 4 and Table 1. The presence of silicon in the matrix of archaeological iron objects is not related to any deliberately addition but it appears as the main element of the Si-rich phases of slag inclusions (SiO_2–rich slags) which formed during production process. The presence of slag in ancient iron is not only due to the ore used but also the smelting system in ancient furnaces, which involved fuel ash, fluxes and furnace lining, as is often suggested in recent literature and reports [31–33]. Chemical compositions of the silver sheet of the hilt was measured by pXRF on three spots and showed that this sheet consisted of silver as a major element and copper as a minor one (Table 1). It shows that the silver sheet has been manufactured from the silver-copper alloy with about 3 wt% of Cu. It may has been added to the silver to increase its strength and hardness [34].

The characterization of the corrosion layer

According to the records of the excavation expedition, current conservation state of the sword is similar to its state when it has been discovered. In addition, all iron swords discovered from this cemetery of the same expedition are similar in the conservation state, the rust layers formed and the surface appearance. Based on available data, it can be derived that the rust crust formed on the surface of the object are due to the burial environment and although the sword has been discovered more than 80 years ago, the effect of display or storage conditions in the rusting process was inefficiently. Relative stability of the sword since its discovery time may be due to two factors: the preventive nature of the outer corrosion layers that were more stable after the mineralization into corrosion products and also controlled storage or display condition in the Egyptian museum. The rust layer and the surface appearance of all iron swords discovered from this cemetery were similar and thus the study of one of these swords may be sufficient to study the characterization of the formed corrosion layers and understanding the corrosion mechanism in this cemetery.

Microscopic observations revealed that the internal corrosion layers of the sword are similar to the corrosion morphologies observed in many iron artifacts buried in the soil environment. The sword was completely covered with a thick corrosion crust mainly constituted of two layers including the internal or the dense product layer (DPL) and the external or transformed medium (TM) (Fig. 5a) [20–22, 35–38]. Based on the literature, DPL layer is an internal corrosion layer formed beside of the metal substrate in which some internal markers such as probable slag inclusions may be visible. It is usually

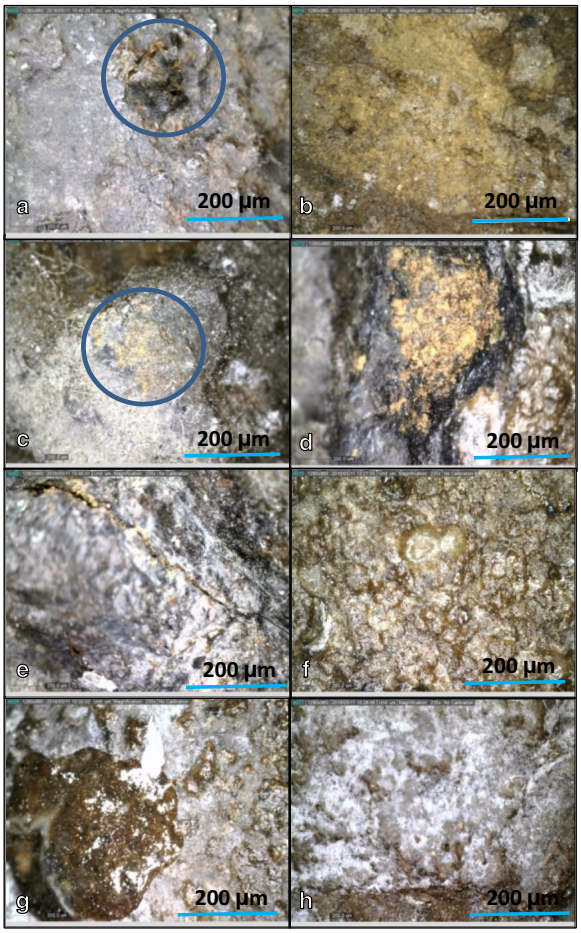

Fig. 3 Stereomicroscope images of the corroded sword surface; **a**–**d** a 'cotton ball' shape of goethite corrosion products, **e** a deep cracks and flaking, **f**, **g** shiny blisters, **h** layer of wax used as protective coating

including oxide/oxyhydroxide iron corrosion products. Furthermore, the TM layer is an external corrosion layer occurring between DPL and non-altered soil in which different iron corrosion products and soil particles are mixed together. The interface between DPL and TM may be the place of the original surface that may have moved during the corrosion events [20, 21].

The characterization of the corrosion layers of the studied sword can be distinguished as following

1. The first layer (DPL); As usual, was observed adjacent to the surface of the metallic structure and is denser than the external layer [39]. The phases of this layer can be distinguished by under optical microscope (OM). The DPL layer is constituted mainly of light yellow phase as a main phase, light marbling strips embedded in the main phase and areas of an orange phase (Fig. 5a–c). Many microcracks as black holes were also observed in this layer. On the other hand, yellow, red and green corrosion spots were observed by OM (Fig. 5d–g), which indicates the probable presence of active corrosion, and thus the sword may be suffered to more corrosion and deterioration in unsuitable conditions.

   Corrosion products of the DPL layer were identified by micro-Raman (Table 2) before the etching; this is important because the etching could alter the corrosion products. Raman spectrum analysis of the light yellow corrosion area, which formed at the most areas of the DPL layer, provided a sharp and high band at 666 cm^{-1} and the next strongest peak at 300 cm^{-1} as in Fig. 6a. These two bands are attributed to magnetite (Fe_3O_4) [20, 35, 40–42]. Furthermore, Raman spectroscopy revealed that discontinuous strips with color of light marbling in the DPL layer are composed of akaganeite (β-FeOOH) mixed with maghemite (γ-Fe_2O_3), Akaganeite is defined at bands 720, 319, 400 and 551 cm^{-1} [43] and maghemite at 720 and 664 cm^{-1} [43, 44], as shown in Fig. 6b. The orange which appears in TM/DPL interface was also analyzed using Raman spectroscopy. The results showed lepidocrocite (γ-FeOOH) as a corrosion product of the orange color detected at a large and intense band at 398 cm^{-1} and various medium bands (139, 209, 338 and 1312 cm^{-1}) (Fig. 6c) [44].
2. The second layer is the transformed medium layer (TM) which has high porosity and has been transformed to the mineralized products. Microscopic examination showed that this layer probably consist of a gray phase mixed with some soil minerals. The gray corrosion phase is the main phase of this layer, Raman spectrum of this phase gave four bands (388 cm^{-1} as the major peak and 299, 549, and 646 cm^{-1} as minor peaks). These corresponded with bands of a goethite corrosion product (α-FeOOH), as shown in Fig. 6d [43–45]. Soil minerals and goethite were observed in the microstructure of this layer by SEM and OM (Fig. 7a–d). Some areas of the outer part of the TM layer are very rich in soil minerals, more than the goethite corrosion, as shown in Fig. 7a, b. The TM layer contains one of the most important decays features of iron artifacts. This phenomenon as known as weeping; the term "weeping" is used for the hollow beads observed in the corroded surfaces of the excavated irons from the soil environment, as shown in Fig. 7e, f [28, 37, 40]. The weeping indicates that the artifact suffered a progressive stage of corrosion under influence of Cl-contamination of

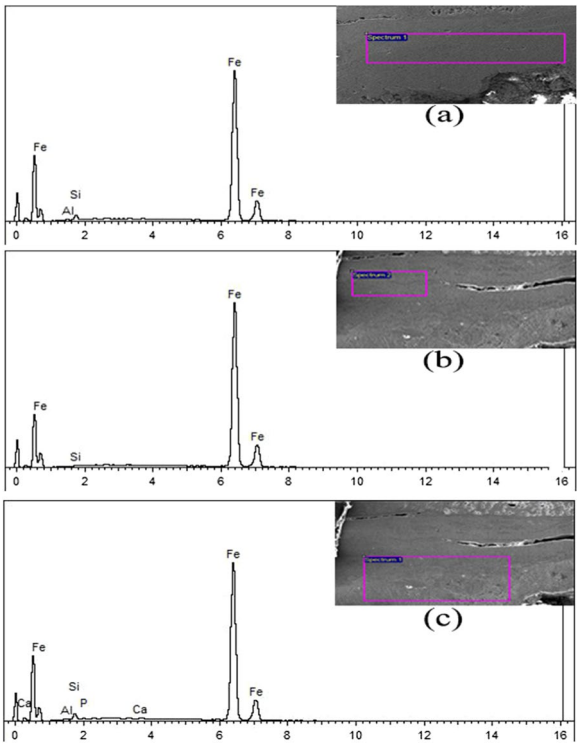

Fig. 4 **a**–**c** EDX analysis of the metallic core of the sword

the object. In some cases, it is considered as a way to determine the authenticity of iron artifacts [28, 40]. The color of this shell was blackish brown and was identified in previous study by Raman spectroscopy as akaganeite [28] and in another one was identified as (α-FeOOH), lepidocrocite (γ-FeOOH) and akaganeite (β-FeOOH) [41].

Elemental analysis by pXRF of thirteen spots on the corroded sword surface showed high concentration of Cl and S (Table 3), and thus there are other corrosion products of the TM layer embedded in the goethite phase. A high concentration of silicon was also detected in several points, with high amount as 63.5, 61.2, 73.5, and 68.4 wt%. Moreover, silicon may be related to quartz which was clearly observed in the microscopic examination by SEM and OM methods (Fig. 7). XRD analysis explained the presence of Cl, S and Si, XRD revealed other iron corrosion products in TM layer including iron sulfate ($Fe_2(SO_4)_3$) and ferric chloride ($FeCl_3$) (Fig. 8). These products often formed in TM layer as a result of the reaction with anions of the soil environment. Also quartz (SiO_2) appeared on the surface as a result of the burial in the soil. It also explains the high percentage of silicon in the corroded sword surface which appeared by pXRF analysis (Table 3). XRD also confirmed the defined products by the Raman and reveals magnetite (Fe_3O_4), goethite (α-FeOOH) and lepidocrocite (γ-FeOOH) (Fig. 8).

The presence of fayalite (Fe_2SiO_4) was also characterized by XRD (Fig. 8). This is a phase formed at high temperature and should not occur due to reaction of the iron with silicon in the soil. Rather, it is clear that this phase originates from the slag inclusions of the metal. The fact that slag inclusions contain fayalite in ancient metals is well known and widely published [32, 33]. The expulsion of slag in ancient smelting furnaces (bloomer furnaces) was never perfect [45]. Therefore, slag inclusions are commonly found in the microstructure of archaeological iron artifacts. The earliest analytical studies of the slag inclusions entrapped in iron were produced in bloomery furnaces [31–33, 46, 47] and revealed a systematic and highly repetitive pattern in slag composition, with most smelting slags plotting in the fayalite region of the FeO–Al_2O_3–SiO_2. Consequently, the crystallized phases inside the slag inclusions were often identified as fayalite and wüstite (FeO) [46, 47].

Table 1 Chemical composition of the sword and the silver sheet

The area	Method	Spectrum	Fe	Si	Al	Ca	P	C	Ag	Cu	AS
The sword	SEM–EDS	Spectrum 1	96	3.2	0.8						
		Spectrum 2	99	0.4							
		Spectrum 3	94	3.6	1.1	0.8	0.4				
	CSA	Spectrum 1						0.4			
		Spectrum 2						0.5			
The silver sheet	pXRF	Spectrum 1							96	2.9	0.3
		Spectrum 2							96	3.2	0.3
		Spectrum 3							97	2.7	0.3

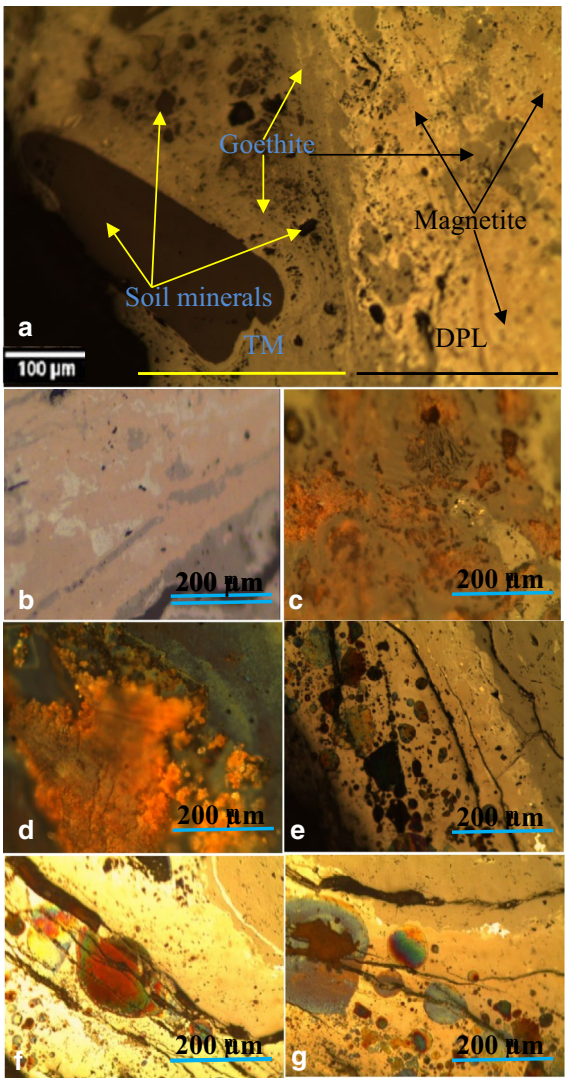

Fig. 5 The cross-section under the optical microscope: **a** the two layers of DPL and TM which can be distinguished based on their colors, **b** light yellow phase as a main phase of DPL layer and the strips of the light marbling phase, **c** areas of an orange phase, **d**–**g** some important aspects of DPL; yellow, red and green corrosion spots as evidence of the active corrosion and many microcracks

The formation mechanism of DPL and TM layer in the studied sword

The corrosion system on the studied sword was formed of two layers; DPL and TM layer. The composition and morphology of the two layers have been summarized in Fig. 9. The DPL is the result of the internal oxidation/corrosion of iron under influence of the burial environment. In fact, The DPL is formed on the metallic substrate by the iron oxidation and its thickness may be variable in different objects from various burial environments. Although, DPL is formed as oxide/oxyhydroxide iron products, it is possible to observe other iron minerals in the composition based on burial environments [20, 21, 48]. The mechanism of formation of the studied DPL layer and its products can be explained as follow: In the beginning of the corrosion process, because high aeration of buried soil, mainly magnetite forms. With the long-term burial and continuous reaction, magnetite layer increased and cracks, parallel to the metal/magnetite interface can form. Burial environment is close to the river Nile and thus the soil is saturated in water. The magnetite layer is connected with the soil and thus its cracks become saturated in water. With the presence of water in the metal/DPL interface, Fe continued to the oxidation to Fe^{2+} and as results of this there are two hypotheses; the magnetite layer increased and other phases formed [20]. Lepidocrocite and maghemite in DPL are a common transformation of magnetite. Some previous studies have indicated that magnetite may alter to maghemite or lepidocrocite [49–52]. Akaganeite formed as results of chlorine in the soil water [20, 22].

The TM is the external corrosion layer in the buried iron objects that is formed by corrosion products which migrated in the pores of the surrounding environment. The thickness of this layer also strongly depends on the corrosively and corrosive of the burial environment (pH, aeration, soluble salts, etc.). In fact, the dissolution of iron and its reaction with surrounding environment may lead to formation and deposition of iron corrosion/oxidation products over the surface of the object, perhaps over the original surface. It is the reason why TM is mixed with the soil particles, in many cases [22, 26, 48]. The formation of goethite product of the studied TM layer attributed to two factors; the formation directly from magnetite with a dissolution/recrystallization pathway and the formation separately as an Fe corrosion product as results of the reaction with Fe^{2+} which migrated

Table 2 The results of micro-Raman analysis

Analysis area	The layer	Raman peaks cm^{-1}	Phase	References
Gray corrosion phase	TM	388, 299, 549, 646	Goethite	[43–45]
Light yellow corrosion	DPL	666, 300	Magnetite	[20, 35, 40–42]
Light marbling corrosion	DPL	720, 319, 400, 720, 664	Akaganeite, Maghemite	[43, 44]
Orange corrosion zone	DPL	398, 139, 209, 338, 1312	Lepidocrocite	[44]

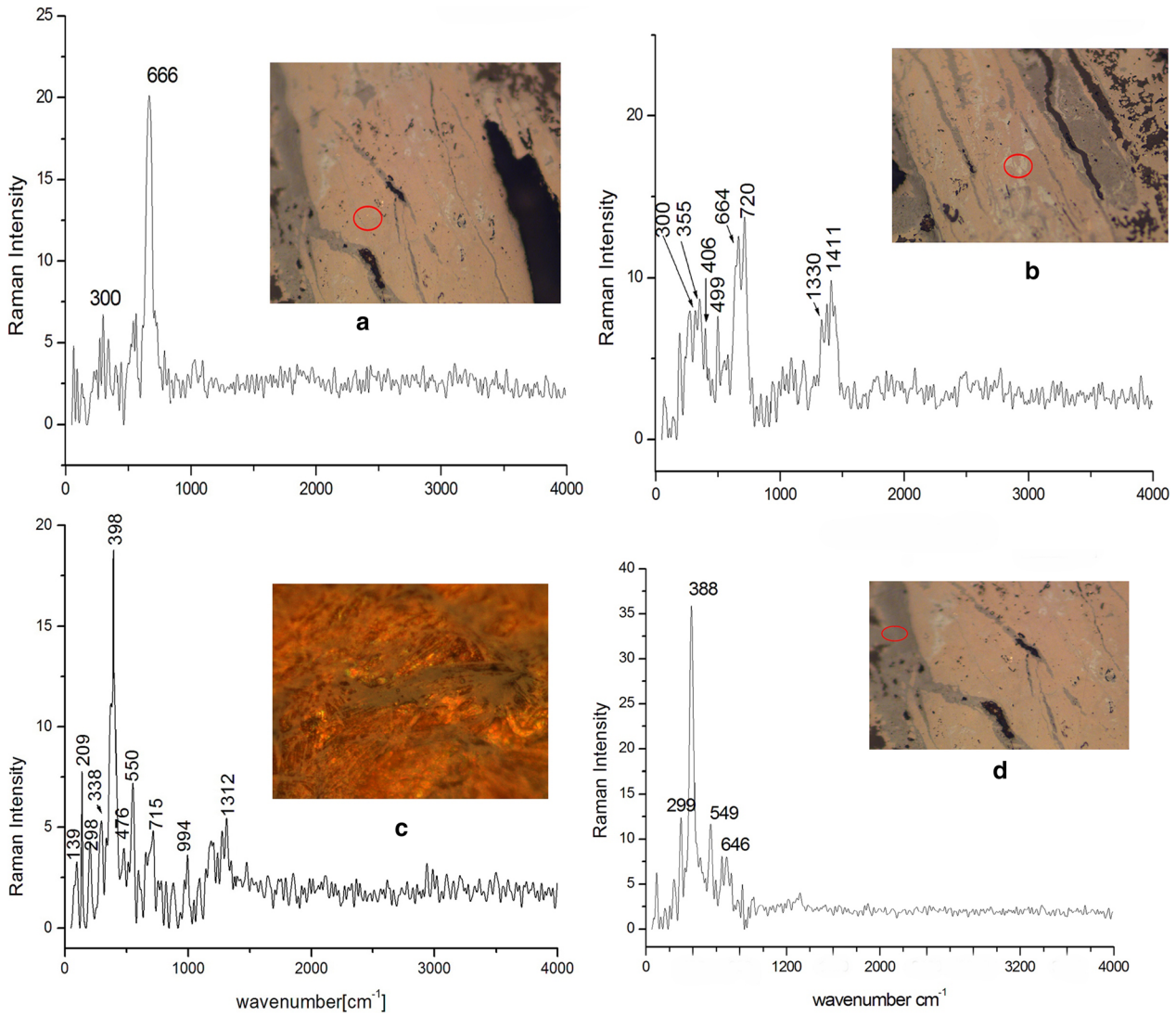

Fig. 6 Representative Raman spectra of the corrosion products of DPL and TM; **a** Magnetite phase, **b** akaganeite and maghemite, **c** lepidocrocite and goethite, **d** goethite phase

from the core through cracks' DPL layer [49, 52, 53]. The corrosion products of iron sulfate ($Fe_2(SO_4)_3$) and ferric chloride ($FeCl_3$) in TM layer formed as a result of the reaction with soil anions such as dissolved ions of sulfate and chloride.

Radiographic investigation

Radiographic examination showed that metallic structure remains only in the middle (internal) zone of the object, and the outer layers are completely transformed into corrosion products. This metallic part retained the sword without large breakings. The study also revealed previous restoration processes such as joining: two pieces appear as separate parts from the sword and are surrounded by a black area as result of the adhesive used which does not appear under X-ray radiation. Furthermore, a fraction was observed in the hilt in the uncovered part with silver. The X-ray investigation also revealed large pores and many gaps were observed as dark areas due to a complete mineralization in these areas (Fig. 10).

Previous and present conservation processes

Previous conservation processes were found on the sword. These include the separated crusts adhered to the sword and the protective coating identified by FTIR, which revealed that the coating is paraffin wax. The

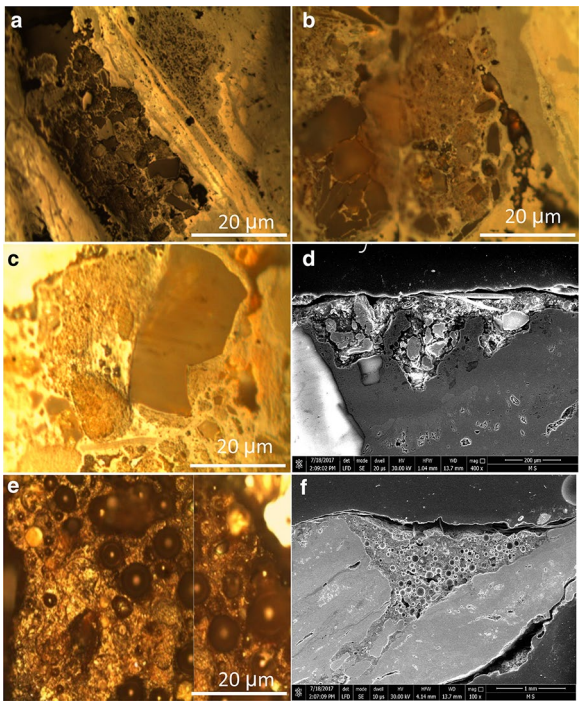

Fig. 7 Metallographic investigation using OM and SEM of the TM layer shows: **a**–**d** the soil minerals (quartz granules) mixed with corrosion products, **e**, **f** the hollow beads indicating weeping

results were compared with the FTIR spectrum of paraffin in a previously published study [54] and also with the analysis result of a standard paraffin sample, as shown in Fig. 11.

The present conservation was carried out in many stages. The first stage is the cleaning process. For metallic artifacts which have been completely or partially exposed to mineralization, there are relatively few conservation choices because the outer layer which includes the details and borders of the original surface is transformed irreversibly into a thick corrosion crust. Therefore, the surface appearance was improved by the removal of thick deposits from the corroded surface. Mechanical cleaning is the sole means to safely remove soil deposit and corrosion products without exposure to chemical solutions [55]. Therefore, the cleaning process was conducted using a dental drilling machine, special fiber glass brushes and scalpels.

The completely or partially mineralized iron artifacts often have the following damage symptoms: weakness in the microstructure, loss in many metallic properties, cracks, swilling, flaking, holes and pores. The filling of cracks and consolidation to secure the surface are necessary. These consolidation processes were performed using a mixture of araldite with oxide of gray color as an adhesive. This mixture was used to fill cracks making the surrounding areas vulnerable to further fracture. Reversibility is a very important principle in conservation so a thin layer of paraliod with oxide of gray color was applied before using the araldite mixture. The final stage was consolidation for protection and stabilization. Paraloid B-44 solution with 3% concentration in ethanol was used to prevent the formation of further corrosion products and improve the stability of the sword [54]. To further protect this sword, it was packed individually and stored in airtight glass box with silica gel; this silica gel should be checked and changed every 3 months until a stable condition is obtained.

Conclusion

The buried iron artifacts in the soil may have been exposed to many agents of decay; therefore, numerous and various chemical and morphological aspects of

Table 3 pXRF analysis of thirteen spots on the corroded surface

No.	Fe	Si	Ca	Ti	K	Mn	Cu	Cl	S
1	33	63	1.5	0.9	0.6	0.2	0.7		
2	34	61	1.7	1.3	1.6		0.1		
3	21	74	1.2	0.9	1.3		0.3		
4	23	73	0.7	0.9	1.2		0.1		
5	30	68	0.4	1. 1					
7	96		0.3	1.7	1.1		0.8		
8	74		0.6	0.4				24	
9	79		0.9		1.9			17	
10	72		1.7	0.4				18	
11	81		1.2	0.4			0.7	16	
12	56		0.7	0.4			0.4	24	18
13	18	46	1.9					17	12

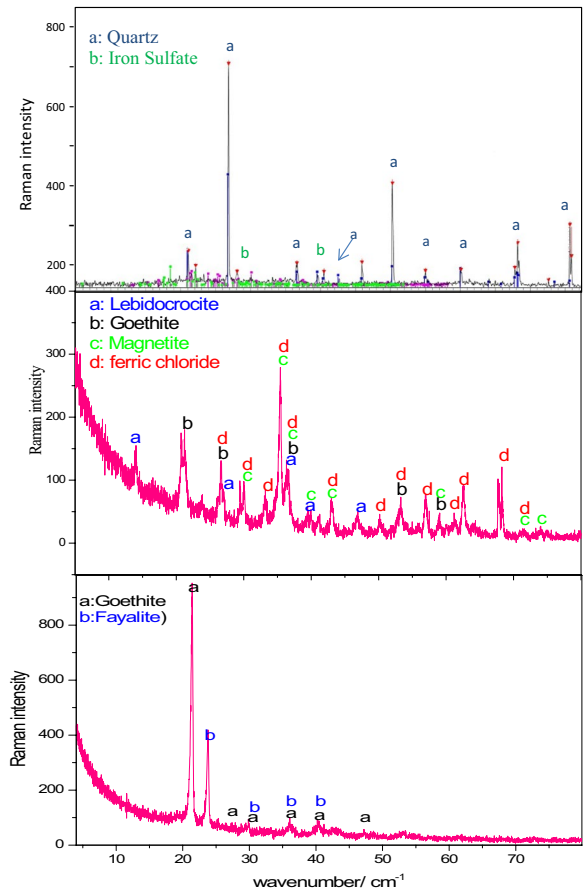

Fig. 8 XRD of three corrosion samples revealed the defined products by the Raman (magnetite, lepidocrocite and goethite), products corrosion did not appeared by Raman (iron sulfate and ferric chloride), slag inclusions of metal (Fayalite)

damage appear on these artifacts. The sword investigated in this paper, is made of low-carbon steel (iron) that has been excavated from a sandy burial soil. It exhibits different types of corrosion. For this purpose, the rust layer covering the residual metal was investigated and characterized by analytical and microscopic methods.

The results of analyses have contributed to understanding the behavior of the object in the burial environment during the long-term abandonment resulting to the formation of the rust on this buried iron artifact. Based on the microscopic, SEM–EDS and XRD studies, the rust crust on this sword consists of two distinct layers: (1) The DPL (dense product layer) which has been covered the remaining metal strucuture, mainly composed of different iron corrosion products including magnetite with some goethite (gray color) and some zones of lepidocrocite (orange color). Numerous cracks are obviously visible in the SEM micrographs of this layer. Also, some yellow, red and green spots were observed in optical microscopy illumination; (2) The TM (transformed medium) layer that its microscopic examination showed that it is constituted of goethite corrosion product mixed with some remnants of the burial environment and some soil minerals such as quartz and calcite. On the other hand, "weeping" was observed as another corrosion aspect in the corrosion crust of the sword. Presence of the weeping as well as small corrosion layers and spots with different colors indicated that the object is suffering active corrosion that shows the conservation problem present in the analyzed sword.

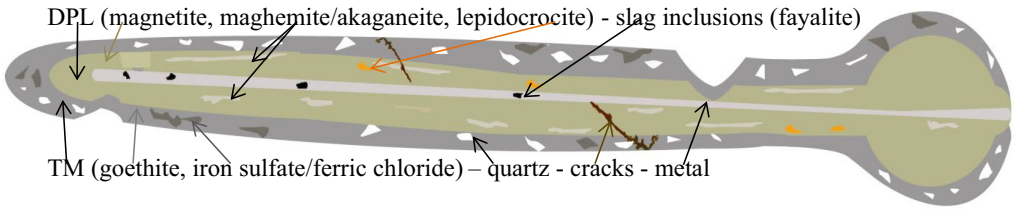

Fig. 9 Schematic description of the corrosion system on the studied sword

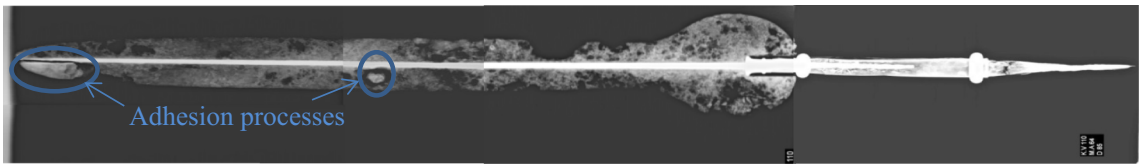

Fig. 10 X-ray radiography reveals that the metallic structure remains only in the middle zone, partially and completely mineralization of the outer edges and previous restoration processes

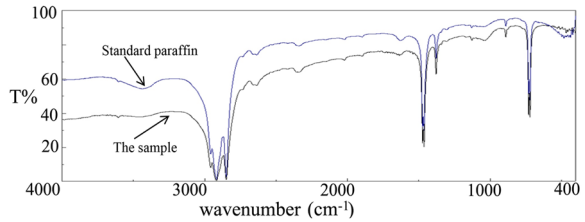

Fig. 11 FTIR analysis of the ancient protective coating were consistent with the FTIR spectrum of and a sample of standard paraffin wax

Finally, based on the results it can be concluded that the corrosion mechanism and morphology observed in the Nubian sword is similar to the corrosion stratigraphy and morphology observed in many archaeological iron objects buried in the soil environment. Presence of two-layered corrosion (rust) crust in this sword covering the metallic structure as well as evidences of active corrosion revealed that the object probably has been buried in a moderate corrosive soil resulting to preserve the metallic structure beneath the DPL and TM corrosion layers. Although, this corrosion stratigraphy and products show partially good conservation conditions occurred in this object, but some evidences of active corrosion revealed that the object needs some specific conservation procedures including RH control and consolidation/stabilization methods. Furthermore, application of various analytical methods in this research showed the importance of scientific studies to characterize the corrosion mechanism and conservation conditions in archaeological iron objects.

Authors' contributions

DO performed the XRF analysis and the Examination by Stereomicroscope. OO added some important paragraphs, read and approved the final manuscript. All other processes were done by YS. All authors read and approved the final manuscript.

Author details

[1] Conservation Department, Faculty of Archaeology, South Valley University, Qena 83523, Egypt. [2] Department of Conservation of Cultural and Historical Properties and Archaeometry, Faculty of Conservation, Art University of Isfahan, Isfahan, Iran. [3] Conservation Laboratory, Egyptian Museum, Giza 12613, Egypt.

Acknowledgements

The authors would like to thank Dr. Mai Rifai Con. Dep. Arch. Fac. Cairo University, for all assistance and support.

Competing interests

The authors declare that they have no competing interests.

Availability of data and materials

All data generated or analyzed during this study are included in this published article and its Additional files.

Funding

Not applicable.

Publisher's Note

Springer Nature remains neutral with regard to jurisdictional claims in published maps and institutional affiliations.

Received: 3 November 2018 Accepted: 19 March 2019
Published online: 28 March 2019

References

1. Hamblin WJ. Warfare in the ancient near east to 1600 BC. New York: Routledge; 2006.
2. Mark JJ. Weapons in ancient Egypt. Ancient history Encyclopedia. 2007. p. 1–9.
3. Loades M. Swords and swordsmen. Great Britain: Pen & Sword Military; 2010.
4. Dan H. Bronze age military equipment. Great Britain: Pen & Sword Books; 2011.
5. Wise T. Ancient armies of the middle east. Oxford: Osprey Publishing; 1981.
6. Comell D, D'orazio M, Folco L, El-Halwagy M, Frizzi T, Albert R, Capogrosso V, Elnagar A, Hassan H, Nevin A, Porcell F, Rashed MG, Valentini G. The meteoritic origin of Tutankhamun's iron dagger blade. Meteor Planet Sci. 2016;51:2–7.
7. Wainwright GA. Iron in the napatan and meroitic ages. Sudan Notes Records. 1945;26:26–36.
8. Rehren T, Belgya T, Jambon A, Káli G, Kasztovszky Z, Kis Z, Kovács I, Maróti B, Martinón-Torres M, Miniaci G, Pigott VC, Radivojevic M, Rosta L, Szentmiklósi L, Nagy ZS. 5,000 years old Egyptian iron beads made from hammered meteoritic iron. J Archaeol Sci. 2013;40(12):4785–92.
9. Johnson D, Tyldesley J, Lowe T, Withers PH, Grady MM. Analysis of a prehistoric Egyptian iron bead with implications for the use and perception of meteorite iron in ancient Egypt. Meteoritics Planetary Sci. 2013;47:997. https://doi.org/10.1111/maps.12120.
10. Dann RJ. The Archaeology of late antique sudan: aesthetics and identity in the royal X-group tombs at Qustul and Ballana. Amherst: Cambria Press; 2009.
11. Walter E. The royal tombs of Ballana and Qustul, vol. I. Cairo: Government Press; 1938.
12. Williams BB. Excavation between abu simbel and the sudan frontier V IX. Chicago: University of Chicago; 1991.
13. Park JS, Gelegdor E, Chimiddor YE. Technological traditions inferred from iron artefacts of the Xiongnu Empire in Mongolia. J Archaeol Sci. 2010;37(11):2689–97.
14. Park JS. A preliminary study on the role and implication of plate-type iron artifacts in the ancient iron technology of Korea. J Archaeol Sci. 2012;39(7):1925–32.
15. Cho NC, Lee HY, Lee JG. Microstructure and heat treatment of early Iron Age cast iron axes excavated from the Sinpung site, Wanju, Jeonbuk, in the Korean Peninsula. Archaeol Anthropol Sci. 2018;8:1–11.
16. Craddock PT. Iron and steel in ancient China: origins and technical change. Antiquity. 1995;68(261):886–90.
17. Starley D. Determining the technological origin of iron and steel. J Archaeol Sci. 1999;26:1127–33.
18. Chen K, Wang Y, Liu Y, Mei J, Jiang T. Meteoritic origin and manufacturing process of iron blades in two Bronze Age bimetallic objects from China. J Cult Her. 2018;30:45–50.
19. Scott DA, Eggert G. Iron and steel in art: corrosion, colorants, conservation. London: Archetype Books; 2009.
20. Neff D, Dillmann Ph, Bellot-Gurlet L, Beranger DG. Corrosion of iron archaeological artifacts in soil: characterisation of the corrosion system. Corr Sci. 2005;47:515–35.
21. Neff D, Reguer S, Bellot-Gurlet L, Dillmann P, Bertholon R. Structural characterization of corrosion products on archaeological iron: an integrated analytical approach to establish corrosion forms. Raman Spectroscopy. 2004;35:739–45.
22. Reguer S, Dillmann Ph, Mirambet F. Buried iron archaeological artifacts: corrosion mechanisms related to the presence of Cl-containing phases. Corr Sci. 2007;49:2726–44.

23. Selwyn LS, Sirois RJ, Argyropoulos V. The corrosion of excavated archaeological iron with details on weeping and akaganeite. Stud Con. 1999;44:217–32.
24. Gerwin W, Baumhauer R. Effect of soil parameters on the corrosion of archaeological metal finds. Geoderma. 2000;96:63–80.
25. Turgoose S. The corrosion of archaeological iron during burial and treatment. Stud Con. 1985;30(1):13–8.
26. Scott DA. Copper and bronze in art: corrosion, colorants and conservation. Los Angeles: Getty Conservation Institute; 2002.
27. Blakelock E, Martinon-Torres M, Veldhuijzen HA, Young T. Slag inclusions in iron objects and the quest for provenance: an experiment and a case study. J Archaeol Sci. 2009;36:1745–57.
28. Wang Q. An investigation of deterioration of archaeological iron. Stud Con. 2007;52:125–34.
29. Antunes RA, Costa I, de Faria DLA. Characterization of corrosion products formed on steels in the first months of atmospheric exposure. Mater Res. 2003;6:403–8.
30. Cano E, Bastidas DM, Argyropoulos V, Fajardo S, Siatou A, Bastidas JM, Degrigny C. Electrochemical characterization of organic coatings for protection of historic steel artifacts. Solid State Electrochem. 2009;3:457.
31. Buchwald VF, Wivel H. Slag analysis as a method for the characterization and provenancing of ancient iron objects. Mater Chara. 1998;40:73–96.
32. Dillmann PH, Balasubramaniam R. Characterization of ancient Indian iron and entrapped slag inclusions using electron, photon and nuclear microprobes. Bull Mater Sci. 2001;24(3):317–22.
33. L'Heritier M, Leroy S, Dillmann PH, Gratuze B. Characterization of slag inclusions in iron objects, chapter in recent advances in laser ablation ICP-MS for archaeology. Berlin: Springer; 2016. p. 213–28.
34. Oudbashi O, Shekofteh A. Chemical and microstructural analysis of some Achaemenian silver alloy artefacts from Hamedan, western Iran. Periodico di Mineralogia. 2015;84(3A):419–34.
35. Grousset S, Bayle M, Dauzeres A, Crusset D, Deydier V, Linard Y, Dillmann Ph, Mercier-Bion F, Neff D. Study of iron sulphides in long-term iron corrosion processes: characterizations of archaeological artifacts. Corro Sci. 2016;112:71.
36. Reguer S, Neff D, Remazeilles C, Guilminot E, Nicot F, Pelé C, Meguelati M, Mirambet F, Dillmann PH, Refait PH, Huet N, Mielcarek F, Rebière J, Bertrand L. Desalinisation of iron archaeological artifacts: understanding of chlorine removal mechanisms of the corrosion layers supported by characterization techniques. Interim meeting of the ICOM-CC metal working group, volume 2: Innovative investigation of metal artifacts. Amsterdam, 2007; p. 60–8.
37. Pingitore G, Cerchiara T, Chidichimo G, Castriota M, Gattuso C, Marino D. Structural characterization of corrosion product layers on archaeological iron artifacts from Vigna Nuova, Crotone (Italy). J Cul Her. 2015;16:372–6.
38. Reguer S, Neff D, Bello-Gurlet L, Dillmann Ph. Deterioration of iron archaeological artifacts: μRaman investigation on chlorinated phases. Raman Spectrosc. 2007;38:389–97.
39. Neff D, Dillmann P, Descostes M, Beranger G. Corrosion of iron archaeological artifacts in soil: estimation of the average corrosion rates involving analytical techniques and thermodynamic calculations. Corr Sci. 2006;48:2947–70.
40. Selwyn L. Overview of archaeological iron: the corrosion problem, key factors affecting treatment, and gaps in current knowledge, proceedings of metal 2004 national museum of australia canberra ACT 4–8 October, 2004. p. 294–307.
41. Saheb M, Neff D, Dillmann Ph, Matthiesen H, Foy E. Long-term corrosion behaviour of low-carbon steel in anoxic environment: characterization of archaeological artifacts. J Nuc Mater. 2008;379:118–23.
42. Ghiara G, Piccardo P, Campodonico S, Carnasciali MM. Microstructural features in corroded celtic iron age sword blades. The minerals, metals & materials society. JOM. 2014;66:793–801.
43. Bellot-Gurlet L, Neff D, Reguer S, Monnier J, Saheb M, Dillmann Ph. Raman studies of corrosion layers formed on archaeological irons in various media. J Nano Res. 2009;8:147–56.
44. Soumya MD, Hendry J. Application of Raman spectroscopy to identify iron minerals commonly found in mine wastes. Chem Geo. 2011;290:101–8.
45. Azoulay I, Conforto E, Refait Ph, Rémazeilles C. Study of ferrous corrosion products on iron archaeological objects by electron backscattered diffraction (EBSD). Appl Phys A. 2013;110:379–88.
46. Mamani EA, Landgrafa FJ, Azevedoa CR. Investigating the provenance of iron artifacts of the royal iron factory of São João de Ipanema by hierarchical cluster analysis of EDS microanalyses of slag inclusions. Mater Res. 2017;4:119–29.
47. Piaskowski J. Metallographic investigations of ancient iron objects from the territory between the oder and the basin of the Vistula River. J Iron Steel Inst. 1961;98:263–82.
48. Neff D, Saheb M, Monnier J, Perrin S, Descostes M, L'Hostis V, Crusset D, Millard A, Dillmann P. Review of the archaeological analogue approaches to predict the long-term corrosion behavior of carbon steel overpack and reinforced concrete structures in the French disposal systems. J Nuc Mater. 2010;402:196–205.
49. He YT, Traina SJ. Transformation of magnetite to goethite under alkaline pH conditions. Clay Miner. 2007;42:13–9.
50. Gilkes RJ, Suddhiprakarn A. Magnetite alteration in deeply-weathered adamellite. J Soil Sci. 1979;30:357–61.
51. Swaddle TW, Oltmann P. Kinetics of the magnetite-maghemite-hematite transformation, with special reference to hydrothermal systems. Can J Chem. 1980;58:1763–72.
52. Xu W, Van der Voo R, Peacor DR, Beaubouef RT. Alteration and dissolution of fine-grained magnetite and its effects on magnetization of the ocean floor. Earth Planet Sci Lett. 1997;151:279–88.
53. Saheb MD, Neff D, Demory J, Foy E, Dillmann P. Characterisation of corrosion layers formed on ferrous archaeological artefacts buried in anoxic media. Corr Eng Sci Technol. 2010;45(5):381–8.
54. Michele D, Stulik RD, Landry JM. Infrared spectroscopy in conservation science. Scientific tools for conservation. Los Angeles: Getty conservation institute; 1999.
55. Bani-Hani M, Abd-Allah R, El-Khouri L. Archeaometallurgical finds from barsinia, northern Jordan: microstructural characterization and conservation treatment. J Cul Her. 2012;13:314–25.

Submit your manuscript to a SpringerOpen journal and benefit from:

- ► Convenient online submission
- ► Rigorous peer review
- ► Open access: articles freely available online
- ► High visibility within the field
- ► Retaining the copyright to your article

Submit your next manuscript at ► springeropen.com